Brain Stimulation 16 (2023) 1722–1732

Contents lists available at ScienceDirect

Brain Stimulation

journal homepage: www.journals.elsevier.com/brain-stimulation

HD-tDCS induced changes in resting-state functional connectivity: Insights from EF modeling

Dario Müller [a,*], Ute Habel [a,b,c], Edward S. Brodkin [d], Benjamin Clemens [a], Carmen Weidler [a]

[a] Department of Psychiatry, Psychotherapy and Psychosomatics, RWTH Aachen University, Pauwelsstraße 30, 52074, Aachen, Germany
[b] JARA-BRAIN Institute Brain Structure-Function Relationships, Research Center Jülich and RWTH Aachen, Germany
[c] Institute of Neuroscience and Medicine 10, Research Center Jülich, 52438, Jülich, Germany
[d] Department of Psychiatry, Perelman School of Medicine at the University of Pennsylvania, 3535 Market Street, Suite 3080, Philadelphia, PA, 19104-3309, USA

ARTICLE INFO

Keywords:
HD-tDCS
Electric field modeling
Resting-state functional connectivity
Interindividual variability

ABSTRACT

Background: High-definition transcranial direct current stimulation (HD-tDCS) holds promise for therapeutic use in psychiatric disorders. One obstacle for the implementation into clinical practice is response variability. One way to tackle this obstacle is the use of Individualized head models.
Objective: This study investigated the variability of HD-tDCS induced electric fields (EFs) and its impact on resting-state functional connectivity (rsFC) during different time windows.
Methods: In this randomized, double-blind, and sham controlled study, seventy healthy males underwent 20 min of 1.5 mA HD-tDCS on the right inferior frontal gyrus (rIFG) while undergoing resting-state functional magnetic resonance imaging (rs-fMRI). Individual head models and EF simulations were created from anatomical images. The effects of HD-tDCS on rsFC were assessed using a seed-to-voxel analysis. A subgroup analysis explored the relationship between EF magnitude and rsFC during different stimulation time windows.
Results: Results highlighted significant variability in HD-tDCS-induced EFs. Compared to the sham group, the active group showed increased rsFC between the rIFG and the left prefrontal cortex, during and after stimulation. During active stimulation, EF magnitude correlated positively with rsFC between the rIFG and the left hippocampus initially, and negatively during the subsequent period.
Conclusion: This study indicated an HD-tDCS induced increase of rsFC between left and right prefrontal areas. Furthermore, an interaction between the magnitude and the duration of HD-tDCS on rsFC was observed. Due to the high EF variability that was apparent, these findings highlight the need for individualized HD-tDCS protocols and the creation of head models to optimize effects and reduce response heterogeneity.

1. Introduction

Non-invasive brain stimulation (NIBS) provides a safe, and non-invasive way to modulate human brain activity and behavior. One NIBS technique is transcranial direct current stimulation (tDCS), which has shown great potential in basic research and applied clinical settings. During tDCS, a weak, direct constant electric current is applied to the scalp via electrodes, alternating the resting membrane potential of neurons [1]. In general, it was found that positive stimulation, the surface inward current, enhances cortical excitability by depolarization of resting membrane potentials, while negative stimulation, the surface outward current, decreases it by hyperpolarization [1]. TDCS can change the excitability of the targeted brain area or network both acutely during the stimulation as well as transiently outlasting the stimulation [2,3]. Long-term effects are due to an increase of neuroplasticity via modulation of glutamatergic synapses, intracellular calcium levels, and NMDA receptors [4–6]. Advantages of tDCS include its comparatively low price, ease of use, and minimal adverse effects. Accordingly, the effects of tDCS are investigated for numerous use cases including clinical applications, modulation of different cognitive functions, emotional processing, and physical performance [7–10].

TDCS interventions also represent an addition to make the treatment of psychiatric and neurological disorders more effective [11]. Here, the right inferior frontal cortex is of interest due to its role in response inhibition [12,13]. Response inhibition is closely associated with cognitive control and executive functioning and deficits constitute a

* Corresponding author. Pauwelsstraße 30, 52074, Aachen, Germany.
E-mail address: darmueller@ukaachen.de (D. Müller).

https://doi.org/10.1016/j.brs.2023.11.012
Received 25 August 2023; Received in revised form 19 November 2023; Accepted 20 November 2023
Available online 25 November 2023

transdiagnostic characteristic for different disorders [14–16]. Considering the recent developments of highly deployable systems in combination with telemedicine technologies, tDCS could be incorporated into digital clinical trials to improve equity of access and overcome methodological barriers [11].

As of now, several obstacles must be tackled before more widespread application of tDCS, particularly in clinical settings, can be achieved. Dichotomous effects of positive and negative tDCS are robust for stimulation over the primary motor cortex, using motor evoked potentials (MEPs) as outcome measures [17], but less so for stimulation of other brain areas such as the prefrontal cortex [17]. Particularly negative tDCS has been shown to induce partially non-linear, dose-dependent neuroplastic effects [18,19]. This points to the problem of high inter- and intra-individual variability in tDCS effects [20,21]. Some studies have demonstrated that even for MEPs, responsiveness to positive tDCS can be as low as 45 % [22]. Multiple factors influence the effectiveness of tDCS. Among them is the duration of the stimulation [23]. Twenty minutes of positive tDCS produced measurable effects that were not apparent in the group receiving 30 min of stimulation [23]. Interestingly, an influence of stimulation intensity was not observed. Other studies do, however, attest to the influence of stimulation intensity [24,25], pointing towards an interaction between the duration and the intensity of the stimulation.

Variability in brain architecture represents another source of heterogeneity in tDCS effects. The distribution of electric fields (EFs) depends on highly individual anatomical features of the head and the brain, such as the thickness of the skull and cerebrospinal fluid, and gyral depth [26]. This is important because the magnitude of the EF and hence the EF magnitude influences tDCS effects [27]. To determine individual EFs, structural magnetic resonance imaging (sMRI) data can be used to create individual head models using the finite element method (FEM). These models help to take the influence of individual brain architecture on induced EFs into account [27–29].

An adapted form of tDCS is high-definition tDCS (HD-tDCS). Compared to conventional tDCS, which is usually applied via two larger electrodes, HD-tDCS uses multiple, smaller electrodes. This allows for better control of how the current is distributed and hence, more focal stimulation. Usually, four to five cathodes are placed in a circle around one centrally placed anode, or vice versa. This reduces unwanted effects exerted by large “reference” electrodes placed over brain regions that are not supposed to be stimulated during conventional tDCS. Also, the possibilities to optimize stimulation parameters and montages are more plentiful using HD-tDCS set-ups. HD-tDCS effects are also thought to last longer compared to conventional tDCS [8], further increasing interest in the technology. On the downside, inter-individual variability in EFs increases with increased focality of the stimulation [30]. Due to the relation between EF magnitude and tDCS effects, this poses a major challenge for the application of HD-tDCS.

One way to better understand HD-tDCS and variability in its effects is resting-state functional MRI (rs-fMRI). It allows investigation of induced changes in functional connectivity (FC) without confounding effects of behavioral differences between individuals [6]. Literature shows that tDCS can modulate large-scale resting-state networks by both increasing and decreasing FC in these networks [31–33]. A systematic review indicated that positive tDCS can also modulate connectivity of the stimulated area with distal, functionally coupled areas [6]. Investigating resting-state functional connectivity (rsFC) during different time windows of receiving tDCS showed a gradual increase of dynamic FC of the stimulated area with the rest of the brain [34]. Another study used fNIRS and a continuous approach [35]. Applying 1 mA of anodal HD-tDCS to the right PFC, it was shown that a gradual increase in the connectivity of this area was significantly reduced after 6 min of stimulation [35]. Findings also revealed that EF variability can predict FC changes in stroke patients [36] and changes in working memory networks of healthy adults [28]. To the best of our knowledge, no study investigated the influence of e-field magnitude on rsFC for different time windows.

This study investigates causes for heterogeneity in HD-tDCS effects, and the influence of potentially increased variability in individual EFs compared to conventional tDCS to inform better protocols for its use. For 20 min, participants received either 1.5 mA HD-tDCS or sham stimulation of the right inferior frontal gyrus (rIFG) during rs-fMRI. We hypothesized that 1.5 mA HD-tDCS would increase FC of this area to the rest of the brain. Based on prior research, we further expected a positive link between EF magnitude and changes in FC and a gradual increase over time.

2. Methods

2.1. Participants

75 healthy, right-handed male participants were recruited using public advertisement (age = 27.3 ± 7.2 years). Exclusion criteria were any contraindications for MRI and any current neurological or psychiatric diseases. Participants were screened for psychiatric disorders before participation using the Structured Clinical Interview for DSM-5 (SCID-5-CV) [37]. The study protocol was in concordance with the Declaration of Helsinki and approved by the internal review board of the medical faculty of RWTH Aachen University. All participants were compensated and gave written informed consent prior to participation. The research project was preregistered at the German Clinical Trials Register (https://drks.de/search/de/trial/DRKS00024471).

2.2. Design

The study employed a randomized, double-blind, and placebo-controlled design. Participants were randomly allocated to either active- or sham stimulation by a person not involved in the measurements. The same person created four different stimulation protocols with the Neuroelectrics Instrument Controller Software (NIC2). Two of these protocols contained the active stimulation and two the sham stimulation. The person conducting the measurement was blind to the content of the protocols and was handed a list of the protocols to use for each participant. Blinding of the participants was assessed at the end of the experiment.

2.3. Blinding and side effects

Blinding success was analyzed with Pearson’s Chi-squared test. Potential side effects were assessed for 12 different categories on a five-point scale ranging from no side effects to strong side effects. The frequency of side effects was assessed with Pearson’s Chi-squared test and dichotomization of variables into either no side effects (option 1) or side effects (options 2–5). The magnitude of side effects was assessed with the Wilcoxon rank sum test.

2.4. Procedure

Participants underwent one MRI session consisting of three separate blocks (Fig. 1). The first block was a resting-state functional MRI (rs-fMRI) measurement of 8 min. Subsequently, participants were taken out of the MRI tube and HD-tDCS was set up using a neoprene cap and saline-soaked sponge electrodes. Participants were put back into the MRI machine and HD-tDCS was started roughly 2½ minutes before the second rs-fMRI block. This time included 30 s of ramp-up. Thereafter, the second rs-fMRI measurement was started and took about 18 min. Before each resting-state session participants were instructed to focus on a white fixation cross on a black background, to not move, to relax, and to let the thoughts run free. Following stimulation, participants were taken out of the MRI tube, the HD-tDCS device was removed, and the last block started. This block consisted of another 8 min rs-fMRI measurement, a T1 weighted and a T2 weighted structural measurement. The time between the end of HD-tDCS and the beginning of the second rs-

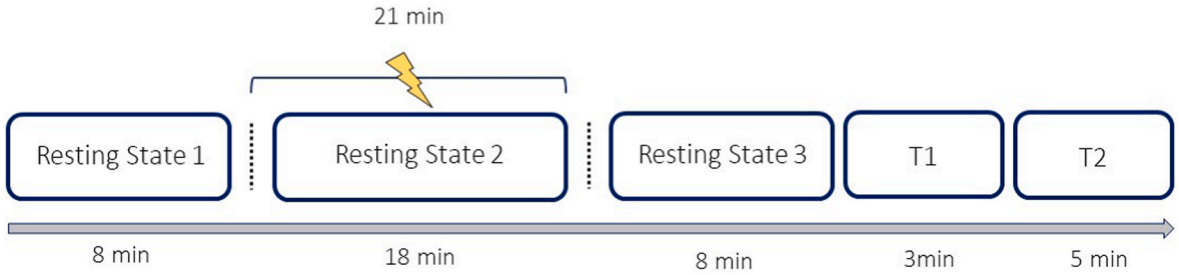

Fig. 1. Procedure of the MRI measurements and HD-tDCS application. *Note.* The time below indicates the time of the magnetic resonance imaging (MRI) sequences. High-definition transcranial direct current stimulation (HD-tDCS) was administered roughly 3 min prior to the second resting-state session for 21 min. Before and after the second MRI measurement, the participant was taken out of the MRI to attach and detach HD-tDCS, indicated by the vertical, dotted lines.

fMRI measurement was five to 10 min. To account for potential head movements between the blocks, the MRI localizer was run again each time participants were taken out of the MRI machine.

2.5. MRI data acquisition

MRI data was collected using a 3-T PRISMA MR scanner (Siemens Medical Systems, Erlangen, Germany) and a 20-channel head coil at the Department of Psychiatry, Psychotherapy and Psychosomatics, Medical Faculty, RWTH Aachen University Hospital.

Resting-state data was acquired using an EPI sequence with 34 slices. In-plane resolution of the slices was 64 × 64 pixels with a total field of view of 192 mm^2 and a voxel-size of 3 × 3 × 3 mm. Images were acquired with a TR of 2000 ms, a TE of 28 ms, and a flip-angle of 77°.

The T1-weighted structural image was acquired using a three-dimensional magnetization-prepared rapid acquisition gradient echo image (MPRAGE) sequence (voxel size: 1 × 1x1 mm, 256 × 256 matrix, FoV: 256 × 256 mm2, 176 slices, TR = 2300 ms, TE = 2.98 ms, flip angle = 9°). The T2 anatomical images were recorded in the same resolution (voxel size: 1 × 1x1 mm, 256 × 256 matrix, FoV: 256 × 256 mm2, 176 slices) and with a TR of 3200 ms and a TE of 417 ms.

2.6. MRI analysis

The following text was automatically generated by the CONN toolbox to enhance transparency and reproducibility.

2.6.1. Preprocessing

Functional and anatomical data were preprocessed using a flexible preprocessing pipeline [38] including realignment with correction of susceptibility distortion interactions, outlier detection, direct segmentation and MNI-space normalization, and smoothing. Functional data were realigned using SPM realign & unwarp procedure [39], where all scans were coregistered to a reference image (first scan of the first session) using a least squares approach and a 6 parameter (rigid body) transformation [40], and resampled using b-spline interpolation to correct for motion and magnetic susceptibility interactions. Potential outlier scans were identified using ART [41] as acquisitions with framewise displacement above 0.9 mm or global BOLD signal changes above 5 SDs [42,43], and a reference BOLD image was computed for each subject by averaging all scans excluding outliers. Functional and anatomical data were normalized into standard MNI space, segmented into grey matter, white matter, and CSF tissue classes, and resampled to 2 mm isotropic voxels following a direct normalization procedure [43,44] using SPM unified segmentation and normalization algorithm [45,46] with the default IXI-549 tissue probability map template. Last, functional data were smoothed using spatial convolution with a Gaussian kernel of 8 mm full width half maximum (FWHM).

2.6.2. Denoising

In addition, functional data were denoised using a standard denoising pipeline [38] including the regression of potential confounding effects characterized by white matter timeseries (5 CompCor noise components), CSF timeseries (5 CompCor noise components), motion parameters and their first order derivatives (12 factors) [47], outlier scans (below 41 factors) [42], session and task effects and their first order derivatives (12 factors), and linear trends (2 factors) within each functional run, followed by bandpass frequency filtering of the BOLD timeseries [48] between 0.008 Hz and 0.09 Hz. CompCor [49,50] noise components within white matter and CSF were estimated by computing the average BOLD signal as well as the largest principal components orthogonal to the BOLD average, motion parameters, and outlier scans within each subject's eroded segmentation masks. From the number of noise terms included in this denoising strategy, the effective degrees of freedom of the BOLD signal after denoising were estimated to range from 220.7 to 259.1 (average 255) across all subjects [43].

2.6.3. First-level analysis

A ROI corresponding to the Magnitude-ROI was manually created using CONN (r = 5 mm, MNI coordinates: x = 50, y = 15, z = 10). Seed-based connectivity maps (SBC) were estimated characterizing the patterns of FC with 165 ROIs. FC strength was represented by Fisher-transformed bivariate correlation coefficients from a weighted general linear model (weighted-GLM) [38], defined separately for each pair of seed and target areas, modeling the association between their BOLD signal timeseries. Individual scans were weighted by a boxcar signal characterizing each individual task or experimental condition convolved with an SPM canonical hemodynamic response function and rectified.

2.6.4. Group-level analyses

Seed-to-voxel group-level analyses were performed using a General Linear Model (GLM) [38]. For each individual voxel, a separate GLM was estimated, with first-level connectivity measures at this voxel as dependent variables (one independent sample per subject and one measurement per task or experimental condition, if applicable), and groups or other subject-level identifiers as independent variables. Voxel-level hypotheses were evaluated using multivariate parametric statistics with random-effects across subjects and sample covariance estimations across multiple measurements. Inferences were performed at the level of individual clusters (groups of contiguous voxels). Cluster-level inferences were based on parametric statistics from Gaussian Random Field theory [38,51]. Results were thresholded using a combination of a cluster-forming $p < 0.001$ voxel-level threshold, and a familywise corrected p-FWE <0.05 cluster-size threshold [52].

2.7. HD-tDCS setup

HD-tDCS was administered inside the MRI using the battery-driven Starstim 8 stimulator (Neuroelectrics, Barcelona, Spain). After a 30-s ramp-up phase, participants in the active group received 20 min of stimulation followed by a 30-s ramp-down phase. Participants in the sham condition received the ramp-up and ramp-down without any

stimulation in between. Resting-state MRI measurements were started after ca. 2½ minutes of stimulation (30-s ramp-up + 120-s of stimulation). HD-tDCS was applied via a 4 × 1 ring setup. An a-priori simulation of the setup was conducted on the "ernie" dataset available at the SimNIBS site (Fig. 2). The anode was placed at F6, and the cathodes at T8, C4, Fp2, and Fz according to the EEG 10–20 system. These coordinates were chosen because the study is embedded in a bigger project that aims to investigate the influence of HD-tDCS of the rIFG on response inhibition. For active stimulation, a current of 1.5 mA at the anode and −0,375 mA at each cathode was used. All electrodes had a circular shape and a radius of 10 mm (3.14 cm^2). The contact between the electrodes and the scalp was established with a sodium chloride solution (NaCl).

2.8. Electric field calculations

EF modeling was done using SimNIBS version 4.0.0[53]. SimNIBS is a comprehensive open-source software that allows the simulation of NIBS-induced EFs. Scripts to automate the analysis were written using the MATLAB toolbox [54]. First, the T1 and T2 weighted images were used to generate individual tetrahedral head meshes using charm, a free SimNIBS module that allows automated tissue segmentation from MR images [55]. Each dataset was inspected to control for the quality of the segmentation with no noticeable problems. Secondly, the electrode setup for each participant was created according to the HD-tDCS setup with the center of the electrodes being defined as their EEG 10–20 coordinate. Electrode and sponge thickness were modeled with 1.5 mm and 2 mm, respectively. Electrode size and sponge size were modeled with a diameter of 20- and 25 mm, respectively. SimNIBS standard conductivity values were used (1). The results of the EF simulations were visualized using gmsh [56], the MATLAB toolbox [54], and the SimNIBS software [26]. The normal component of the EF for each tetrahedron was averaged across all participants. The standard deviation (SD) of each tetrahedron across all participants was also calculated. The data was plotted with different percentile thresholds on a template brain to visualize the mean EF and the SD. Additionally, the normal components of individual EFs were calculated and plotted with different percentile thresholds. In the last step, the mean EF magnitude for each participant in a manually created region of interest (ROI) of a 5 mm radius was calculated. The ROI was centered around the MNI coordinates (x = 50,y = 15,z = 10) and will be called *Magnitude-ROI* in the following text. The coordinates were chosen because they correspond to the area that was aimed to be stimulated, the rIFG. SimNIBS allows the transformation of MNI space to the head model of the individual subject using the mni2subject command.

To compare the e-fields of our setup with a conventional setup, we also simulated a conventional setup with equal parameters. We used the same anode and a contralateral, elliptical return electrode at F with the same thickness and an electrode and sponge diameter of 60- and 65 mm, respectively.

2.9. MRI analysis

Results included in this manuscript come from analyses performed using CONN [57] (RRID:SCR_009550) release 21.a [58] and SPM [59] (RRID:SCR_007037) release 12.7771. Five participants had to be excluded from the analysis, leaving 70 participants in the sample. Participants were excluded due to a significant brain anomaly under the electrode (n = 1), equipment failure in the middle of the stimulation (n = 1), and due to insufficient data quality (n = 3). Rs-fMRI data was divided into five different conditions. The first and the last rs-fMRI measurements were entered as pre- and post-measurement, respectively. The third measurement, with simultaneous HD-tDCS administration, was divided into three equal parts: *Stimulation 1* (2–8 min of stimulation), *Stimulation 2* (8–14 min of stimulation), and *Stimulation 3* (14–20 min of stimulation).

2.10. Functional connectivity analyses

A ROI corresponding to the *Magnitude-ROI* was manually created using CONN (r = 5 mm, MNI coordinates: x = 50, y = 15, z = 10). Seed-based connectivity maps (SBC) were estimated characterizing the patterns of FC with 165 ROIs based on the Harvard-Oxford atlas [60]. Seed-to-voxel group-level analyses were performed using a General Linear Model (GLM) [38]. Results were thresholded using a combination of a cluster-forming $p < 0.001$ voxel-level threshold, and a familywise corrected p-FWE <0.05 cluster-size threshold [52]. Plots were created with R [61] and the ggplot2 package [62].

Active vs sham stimulation. In the first analysis, the effects of HD-tDCS on rsFC were investigated. Participants were grouped in an active (n = 36) and a sham (n = 34) group. Two different seed-to-voxel

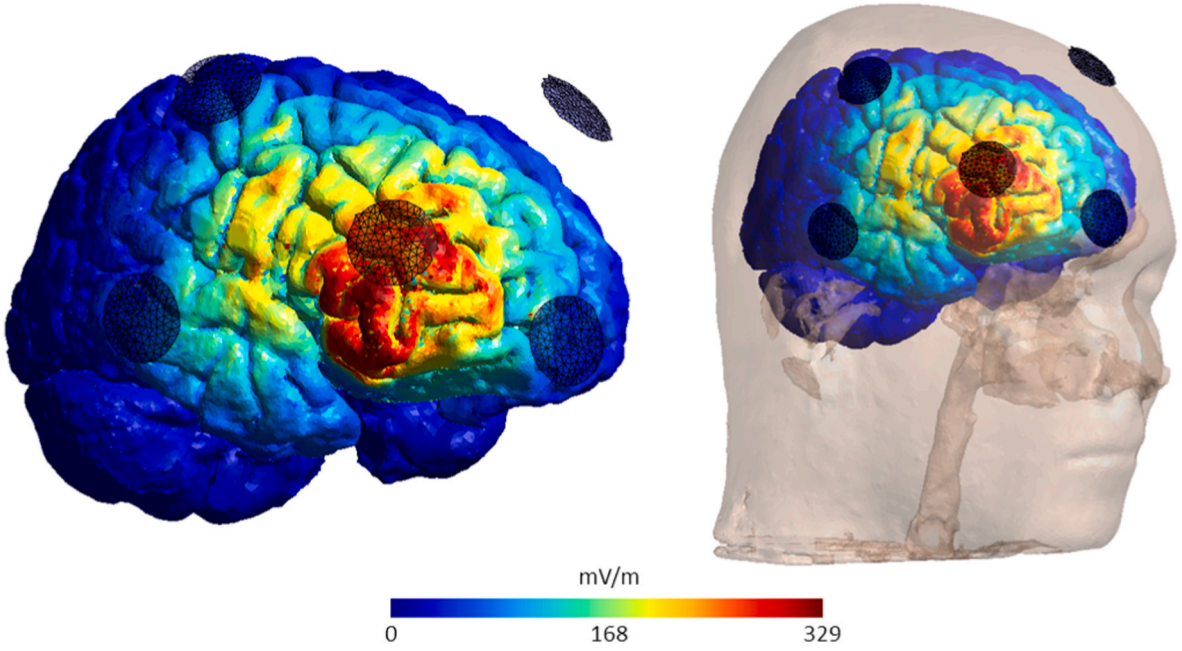

Fig. 2. A priori simulation of the electric field distribution. *Note.* The simulation was conducted on the "ernie" template brain provided by SimNIBS.

analyses were performed; one with the *Magnitude-ROI* as seed region, and one with the rIFG pars triangularis (rIFG-ptr). The rIFG-ptr was chosen because it showed the highest mean EF magnitude. The *Magnitude-ROI* was chosen to augment the analysis of the effects of EF magnitude on rsFC. For both analyses, the effect of HD-tDCS on *Stimulation 1*, *Stimulation 2*, *Stimulation 3*, and *Post-Stimulation*. was analyzed with a 2 × 4 (stimulation x session) repeated-measures analysis of variance (ANOVA) followed by post-hoc t-tests. Lastly, potential baseline differences between the active and sham conditions were tested for in both analyses.

Effects of e-field magnitude. For the sub-analysis in the active tDCS group, a seed-to-voxel analysis for the effect of individual EF intensities on rsFC was calculated (n = 36). The effect of EF intensities on rsFC during stimulation was investigated with a multiple regression F-Test for the three different time windows (*Stimulation 1*, *Stimulation 2*, *Stimulation 3*), followed by post-hoc t-tests. The same test was conducted in the sham group as a sanity check.

3. Results

3.1. Seed-based resting-state fMRI analysis

An overview of all analyses can be found in Table 1. The resting-state measurement was divided into three time windows of 6 min each. Before the first-time window, the participants received 30 s ramp-up followed by 20 min of active stimulation.

3.1.1. Effects of HD-tDCS on resting-state functional connectivity

In the first analysis, differences in rsFC between the active- (N = 36) and the sham group (N = 34) were analyzed. Two seed-to-voxel analyses were conducted, one with the *Magnitude-ROI* as a seed, and the other with the rIFG-ptr. Inspections of baseline differences between groups yielded no significant results. In the second analysis, a seed-to-voxel analysis of the *Magnitude-ROI* with EF magnitude as a covariate was conducted.

Right inferior frontal gyrus, pars triangularis. Active > Sham. Seed-based FC analysis showed a significant effect of stimulation x session (p-FWE = 0.0002) on rsFC between the rIFG-ptr and a cluster including the left frontal pole (K = 106), the left middle frontal gyrus (K = 69) and the left IFG-ptr (K = 26) (Table 1 and Fig. 3). Post-hoc t-tests revealed significantly increased connectivity in the active as compared to the sham group during *Stimulation 1*, t (68) = 2.12, p = 0.038; *Stimulation 2*, t (68) = 2.29, p = 0.025; and *Post-Stimulation*, t (68) = 4.71, p < 0.0001. No significant differences were found during *Stimulation 3*, t (68) = 0.06, p = 0.47. After Bonferroni correction for multiple tests, only *Post-Stimulation* remained significant.

Table 1
Effects of high-definition transcranial direct current stimulation on resting-state functional connectivity.

Stimulation x session, (N = 70), active > sham				
Seed	*Clusters (k)*	*Anatomical region*	MNI *peak voxels (x, y, z)*	*FWE*
Magnitude-ROI	*No significant cluster (p-FWE > 0.077)*			
R Inferior Frontal Gyrus Pars Triangularis	226	L Frontal Pole (K = 106)	−46, 40, 16	p = 0.0002
		L Middle Frontal Gyrus (K = 69)	−46, 34, 22	
		L Inferior Frontal Gyrus Pars Triangularis (K = 26)	−48, 34, 16	
		L Non-labeled (K = 25)	−50, 40, 18	

Post-hoc t-test			
Contrast	*beta*	*t*	*p (two-sided)*
tDCS active > tDCS sham (during stimulation 1)	0.110	2.12	0.038
tDCS active > tDCS sham (during stimulation 2)	0.120	2.29	0.025
tDCS active > tDCS sham (during stimulation 3)	0.003	0.06	0.949
tDCS active > tDCS sham (post-stimulation)	0.230	4.71	<0.0001

Note. R, right; L, left; FWE, family wise error; MNI, Montreal Neurological Institute. Post-Hoc t-tests for functional connectivity between the seed regions and the significant clusters found during the analyses.

3.1.2. Effects of current density on functional connectivity

In the active group (N = 36), the mean magnitude of the EFs inside the *Magnitude-ROI* was 145.8 mV/m (±30.5). Seed-based FC analysis showed significant differences in rsFC between the seed and a cluster centered around the left hippocampus (K = 89, p-FWE = 0.039; Table 2 and Fig. 4). Post-hoc t-tests revealed that EFI was linked positively to rsFC during the first time window and negatively during the second one (Table 2). During the third time window of active stimulation, the negative impact of EFI on rsFC was not significant. For comparison, the influence of EFI was also tested in the sham group with no significant results. Seed-based FC analysis of active > sham independent of the EF magnitude showed no difference in rsFC between the groups.

3.2. Electric field modeling

3.2.1. HD-tDCS

Simulated EF distributions and their SDs for all subjects are presented in Fig. 5. The normal component of the EF located in the rIFG-ptr was approximately 200 mV/m. Nevertheless, areas including the superior temporal gyrus, the middle frontal gyrus, and the precentral gyrus also showed EFs in the upper percentile (see Fig. 5 & Table 3). The orientation of the gyrus to the electrode also appears important, with areas facing the anode showing higher EFs compared to areas facing away from it. The ratio of EF normal components to their SD decreases with an increase in the percentile thresholds (i.e.: the SD at the 50th percentile threshold is higher compared to the mean at the same threshold than it is at the 90th percentile threshold). The EF for all participants at different percentiles can be seen in Table 3 and Fig. 6. The figures display the mean EF for all tetrahedrons in the brain.

3.2.2. Conventional tDCS

Simulated EF distributions and their SDs can also be seen in Fig. 5. The simulations indicate higher-, and more distributed EFs compared to the HD-tDCS setup, with considerable spread to the contralateral side towards the return electrode. Similar to the HD-tDCS setup, the EF peak is located at the rIFG-ptr, with the additional inclusion of the pars orbitalis.

3.3. Blinding and side effects

Most participants tolerated the stimulation well and there was no significant difference between groups for selection of active or sham [χ [2] = 0.53 (1), p = 0.47]. In the active group, 86 % believed they had received real stimulation compared to 77 % in the sham group. No difference in magnitude or frequency of any side effects was observed between groups. A detailed overview can be seen in the Supplement 2. The only group difference was found in the duration of the sensation, with 12 participants reporting side effects during the whole stimulation, 10 of them having received active stimulation.

4. Discussion

The current study examined HD-tDCS effects over the rIFG on rsFC. We further investigated variance in HD-tDCS EF distribution and its influence on rsFC during different stimulation time windows. Analyses demonstrated substantial variance in induced EFs and increased rsFC during active compared to sham stimulation. The analysis also revealed a relation between EF magnitude and changes in rsFC between the rIFG

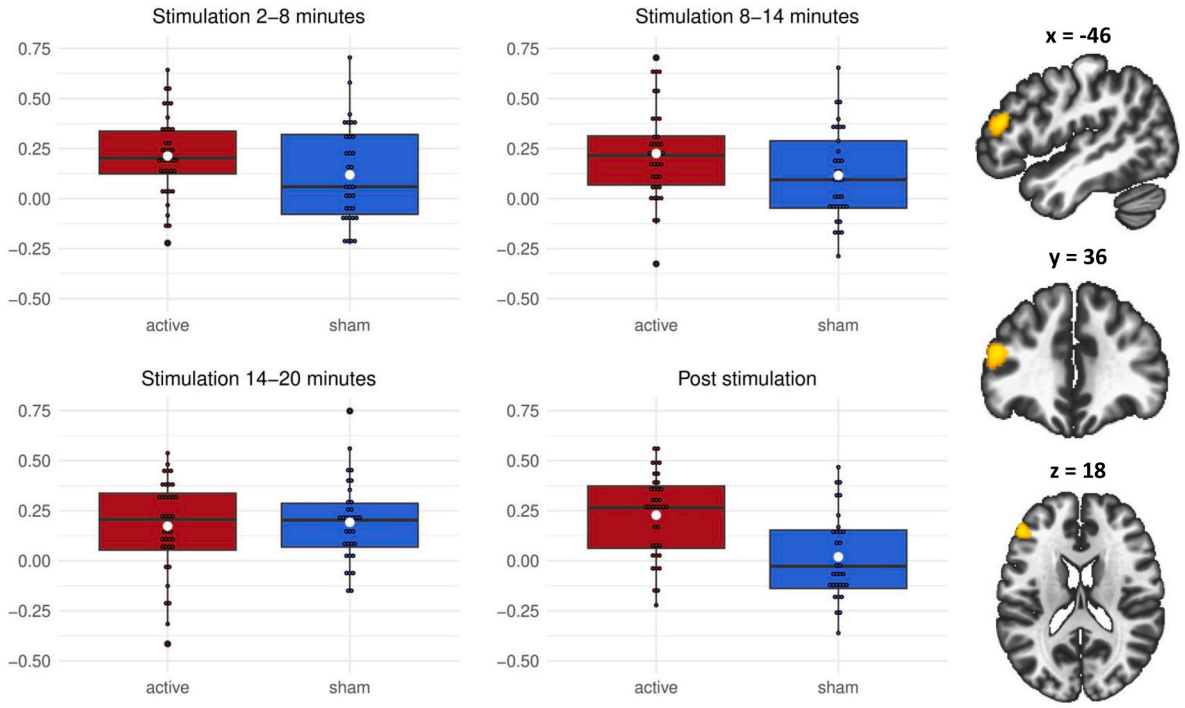

Fig. 3. Significant main effect of HD-tDCS on resting-state functional connectivity shows increased connectivity between the rIFG pars triangularis and the cluster highlighted in the pictures, active > sham. *Note.* Boxplots depicting the active- and sham group on the x-axis, and fisher transformed correlation on the y-axis. Fisher transformed correlations relate to the BOLD timeseries correlation between the rIFG pars triangularis and the significant cluster that was found in the analysis. The brains on the right depict the significant cluster that was found in the analysis.

Table 2
Effects of e-field magnitude on resting-state functional connectivity.

Electric field magnitude x session, (N = 36)				
Seed	*Clusters (k)*	*Anatomical region*	*MNI peak voxels (x, y, z)*	*FWE*
Magnitude-ROI	89	L Hippocampus (K = 72) L Amygdala (K = 2) L Non-labeled (K = 15)	−26, −20, −16 −28, −10, −16 −28, −16, −12	p = 0.039

Post-hoc t-test			
Contrast	*beta*	*t*	*p (two-sided)*
Effect of electric field magnitude (during stimulation 1)	2.09	3.23	0.003
Effect of electric field magnitude (during stimulation 2)	−2.53	−2.96	0.006
Effect of electric field magnitude (during stimulation 3)	−1.32	−1.62	0.114

Note. R, right; L, left; FWE, family wise error; MNI, Montreal Neurological Institute. Post-Hoc t-tests for functional connectivity between the seed regions and the significant clusters found during the analyses.

and the left hippocampus providing preliminary evidence for a change in direction of this relation during stimulation.

4.1. Effects of HD-tDCS on rs-fMRI

Compared to the sham group, the active group showed increased rsFC of the rIFG-ptr to a cluster in the left PFC during the first two parts of stimulation, and directly after. The latter was more prominent in that the difference in the first two parts did not survive Bonferroni correction. The cluster included the frontal pole, the middle frontal gyrus, and the IFG-ptr. Our findings show that HD-tDCS effects are not limited to resting-state networks but affect functionally coupled areas distant from the stimulation site.

Observed increases in connectivity coincide with the idea of enhanced cortical excitability through positive tDCS [1,6]. Evidence for FC between these areas comes from theta burst stimulation to the left IFG being associated with increased activity in the rIFG [63]. Literature on the influence of HD-tDCS on rsFC is more limited. Combining fNIRS and HD-tDCS of the right PFC, revealed FC increases between the stimulated area and the corresponding contralateral area [64]. Other studies, however, paint a more heterogeneous picture showing that positive tDCS can lead to both increased- and decreased rsFC [31,64,65]. In our study, rsFC differences during stimulation were mainly driven by fluctuations in the sham group, whereas rsFC remained stable in the active group. RsFC indeed presents temporal variability attributed to noise but also to natural temporal dynamics [66,67]. This poses an interesting viewpoint, the stabilization of rsFC through HD-tDCS. Anomalies in rsFC are present in various mental disorders [68–70] and pose an interesting target for tDCS interventions. Here, prefrontal areas such as the inferior frontal gyrus are the main targets for psychiatric interventions. In combination with EF models, our results can help to inform the individualization of future (HD-)tDCS protocols. Lastly, our findings also indicated the biggest difference in rsFC between active and sham after stimulation, but little information is available on online vs. offline HD-tDCS effects on rsFC. HD-tDCS studies with behavioral endpoints indicate that effects are most prominent around 30 min after stimulation, fitting with our observation [8].

The second seed-to-voxel analysis including the *Magnitude-ROI* as the seed did not show significant group differences. This is interesting considering the link between EF magnitude and rsFC that was found in this region. A potential reason might be the lower EF magnitude compared to the rIFG-ptr as well as the higher variability that was associated with it.

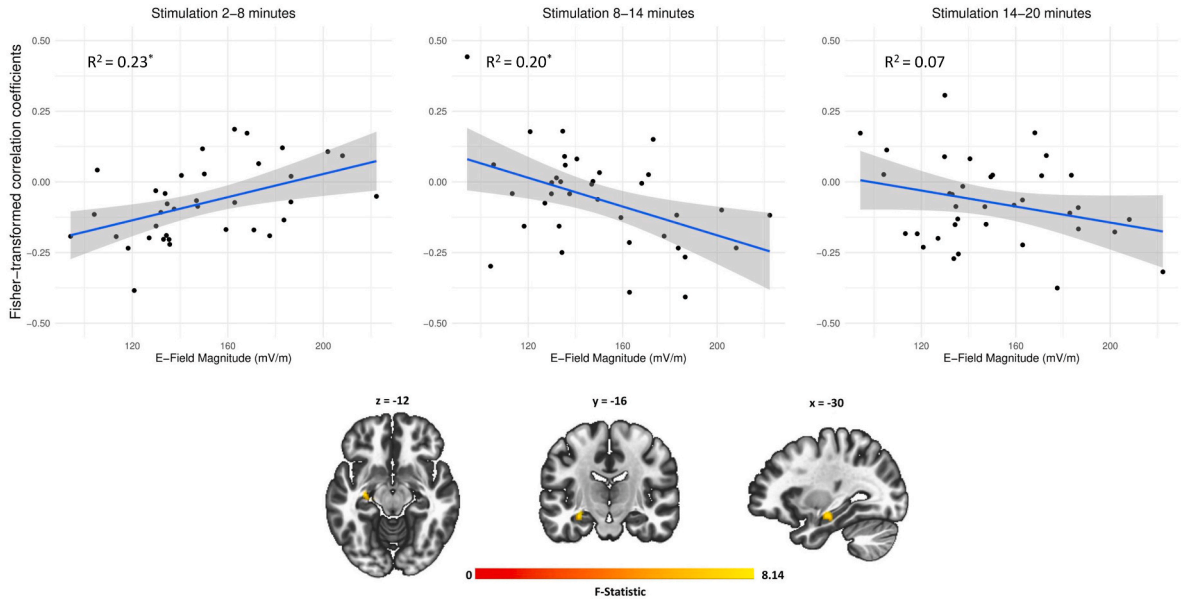

Fig. 4. Effects of electric field magnitude on functional connectivity between the Magnitude-ROI and the significant cluster. *Note.* Correlation plots between electric field magnitude on the x-axis, and fisher transformed correlation on the y-axis. Fisher transformed correlations relate to the BOLD timeseries correlation between the spherical 5 mm seed region and the significant cluster that was found in the analysis. The brains on the right depict the significant cluster that was found in the analysis.

4.2. Effect of electric field magnitude on functional connectivity

To our knowledge, this is the first study to explore the effects of EF magnitude on rsFC during different time windows. Our results indicate a specific influence of EF magnitude on rsFC between the *Magnitude-ROI* and parts of the hippocampus. During the first stimulation window, low EF magnitudes related to reduced FC while higher magnitudes were associated with slightly increased connectivity. Interestingly, this relationship was reversed during the second stimulation window. For the last part, the direction of the relationship was still negative but insignificant. A recent fNIRs study indicated a significant reduction of a tDCS-induced increase in connectivity of the right PFC after 6 min of stimulation, but no reversal of this relationship [35]. Other studies indicate lower EF magnitudes to be linked to increased, and higher intensities to decreased FC for negative tDCS [71]. In general, the reversal of tDCS effects on cortical excitability is a known phenomenon but normally occurs after much longer stimulation [72,73]. The fast switch in the relation between magnitude and changes in rsFC we observed is rather surprising and suggests an interaction between stimulation duration and EF magnitude. A recent study found an interaction between stimulation intensity and time but only after 26 min of stimulation, likely relying on counter-regulatory mechanisms [73].

A potential explanation could be a state-dependent interaction between rsFC and EF-magnitude. Our EF simulations are based on anatomical information and therefore assume a static electric field, treating the brain as an inanimate object. Hence, the model cannot account for any interaction between the electric field and the dynamic brain state which might mediate the influence of EFs on rsFC. On a behavioral level, tDCS effects are indeed shown to differ according to baseline performance [74]. Using EEG, it could also be shown that baseline amplitudes of event-related potentials condition tDCS induced changes of those [75]. Notably, our explorative whole-brain approach warrants future investigation of this interaction with a priori-defined brain areas and task-based studies. If replicated, this finding holds implications for the appropriate duration and intensity of stimulation in future (HD-)tDCS studies. Literature indicates lower EF intensity in some patient groups when compared to healthy controls [76], creating a potential source of response heterogeneity.

4.3. Electric field modeling

We applied 1.5 mA HD-tDCS to the rIFG. The highest EF magnitude was observed at the rIFG-ptr. Nevertheless, areas including the superior temporal gyrus, the middle frontal gyrus, and the precentral gyrus also showed a high EF magnitude. While comparison with the simulation of the conventional set-up showed that HD-tDCS is more focal, isolating single gyri remains challenging. Both conventional and HD-tDCS simulations showed the highest EF at the IFG, with conventional tDCS producing higher EF magnitudes. The results also indicated considerable variation in EFs for both conventional and HD-tDCS. For HD-tDCS, the area that experienced the highest EF also showed the highest inter-individual variance while for the conventional setup, this shifted towards the return electrode. For a substantial part of tetrahedrons in both simulations, variability was so high that an EF magnitude of zero mV/m fell within one SD of the mean EF magnitude (Supplement 3). The mean EF magnitude to SD ratio decreased with higher percentile thresholds, being lowest at the tetrahedrons with the highest EF magnitude. Interestingly, EF analysis of the *Magnitude-ROI* shows a smaller mean-to-SD ratio for larger, functionally important areas. This suggests that the smaller the targeted area, the higher the variability and hence, the more heterogeneous the effects. Based on the observed influence of EF magnitude on rsFC, high EF variance emphasizes the importance of a priori EF simulation, especially for HD-tDCS setups. Further evidence comes from a recent study that applied conventional tDCS during an n-back task. Here, the current density in the left dorsolateral PFC correlated positively with the functional connectivity of this area [28]. These findings might be transferred to behavioral endpoints. Utilizing multiple sessions of conventional tDCS during a cognitive training intervention, treatment response was predicted by individual EFs [27].

4.4. Model validity

EF field models were based on individual headmodels. These were created with charm, an automated tissue segmentation method that has been shown to increase the accuracy of EF simulation when compared to other methods [55]. Both T1-and T2-weighted anatomical images were used to further improve the validity of the head models. Each

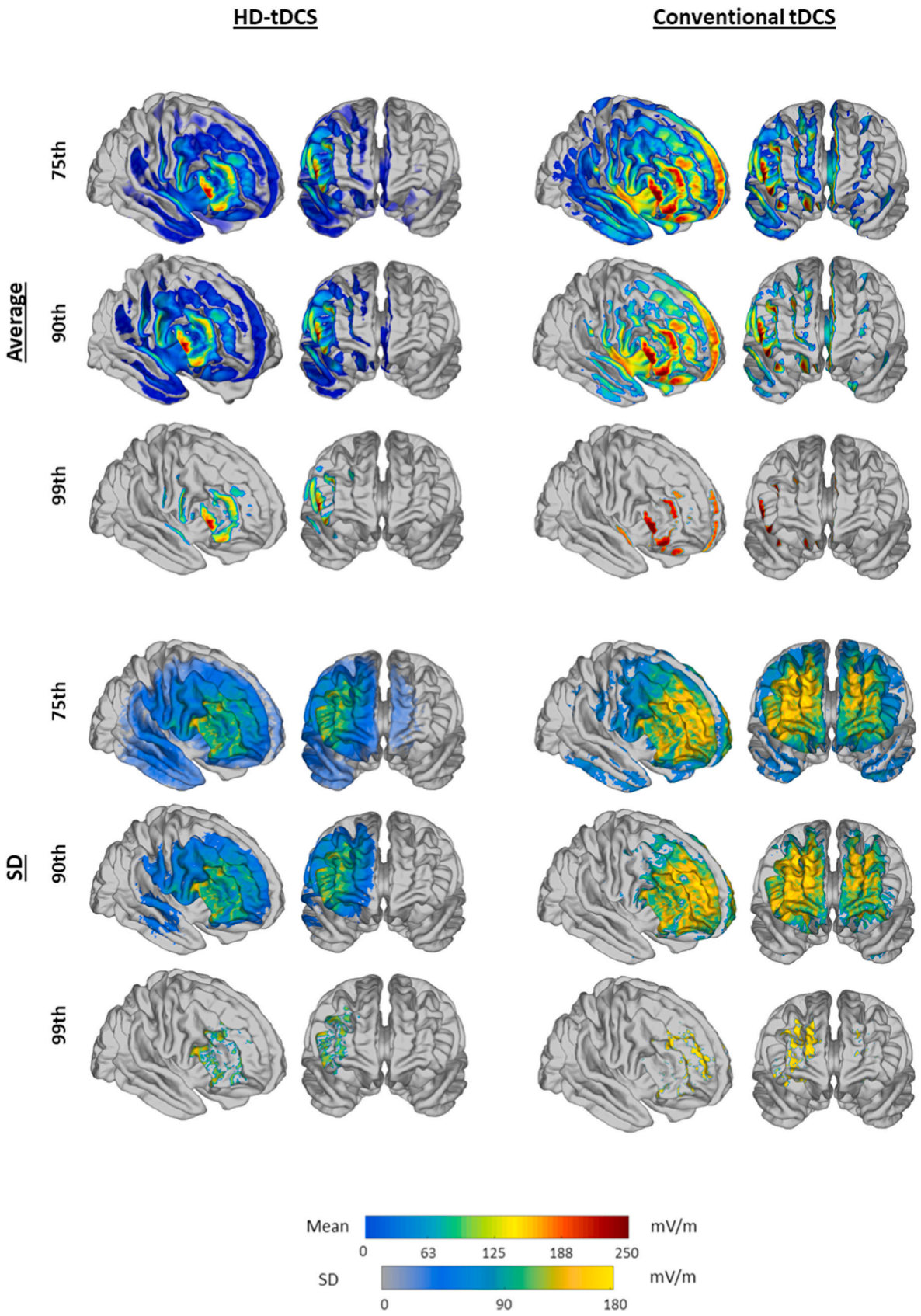

Fig. 5. E-field distributions at different percentile thresholds. *Note.* The left side shows the simulation of the HD-tDCS setup that was used for the experiment. The right side depicts a simulation of a conventional setup for comparison.

Table 3
Electric field magnitude for different percentile thresholds.

Percentile Thresholds	HD-tDCS		Conventional tDCS	
	Mean	Standard Deviation	Mean	Standard Deviation
50th Percentile	−1.8	8.9	0.0	42.3
75th Percentile	5.4	17.7	34.5	61.4
90th Percentile	20.9	39.9	80.4	95.3
95th Percentile	39.6	65.2	113.0	122.2
99th Percentile	87.1	104.2	177.7	160.5
99.9th Percentile	148.9	124.8	227.5	188.3

Note. All values are presented in mV/m. The mean values present the percentile thresholds after averaging each tetrahedron over all participants.

segmentation was visually checked for discrepancies between the T1 reference volume and assigned tissue labels. Except for minor issues (e.g.: nose not completely included in the segmentation), no problems were encountered and hence, no manual changes were conducted.

To foster accurate placement of the electrodes, standardized caps designed after the EEG 10–20 system were used. The size of the cap was adapted to the head circumference of the participant and centering of the cap was ensured by individual measurement of standard reference points, i.e.: ear-to-ear and nasion to inion. The same EEG 10–20 coordinates were then used in SimNIBS to simulate the e-field. In a pilot sample, we did not observe discrepancies between simulated-, and actual placement of the electrodes. Still, for the e-field simulation in our study we relied on the presumed location of the electrodes, and due to factors like hair and human error, slight discrepancies between simulated-, and actual electrode placement might have arisen. These discrepancies can translate to discrepancies between simulated-, and actual e-field which could have negatively impacted the validity of our models.

4.5. Limitations

A potential limitation is the time of the resting-state measurements. Pre- and post-measurements were shorter compared to the measurement with simultaneous HD-tDCS stimulation, which was long compared to standard rs-fMRI protocols. Evidence suggests however that even 24 min of rs-fMRI does not reduce the reliability of rsFC measures [77] and the difference in duration was tried to be compensated for by dividing the measurement with simultaneous stimulation into different time windows with a duration similar to the pre- and post-measurements. Still, it

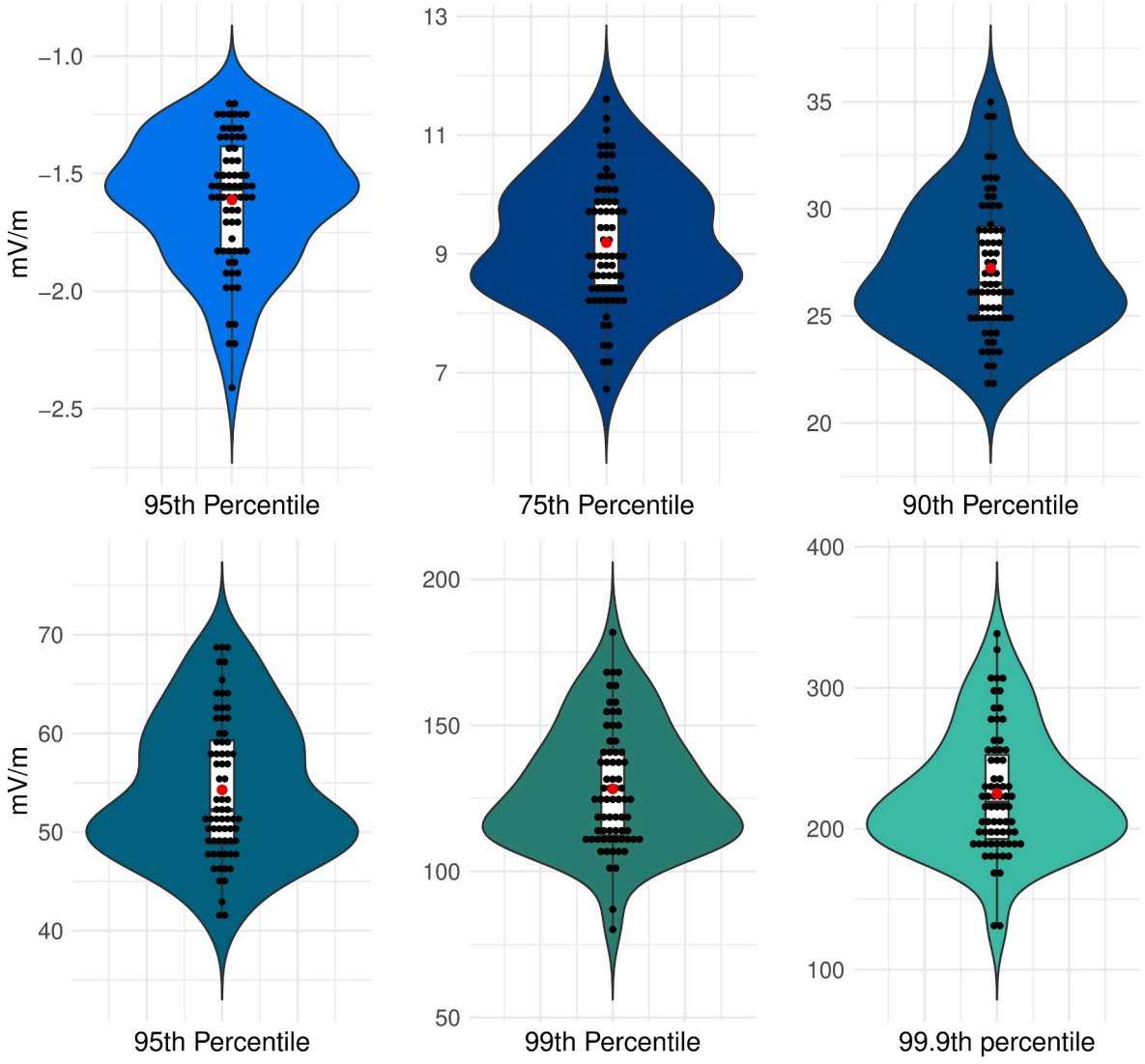

Fig. 6. Electric field magnitude of each participant for different percentile thresholds. *Note.* The Y-Axis represents the electric field magnitude. The corresponding percentiles are shown under the violin plots. Black dots represent individual electric field values for the respective percentile threshold. The red dot shows the mean for each percentile threshold over all participants. All values are calculated for the whole brain. (For interpretation of the references to colour in this figure legend, the reader is referred to the Web version of this article.)

creates a potential confounder for the interpretation of the results.

Another potential concern is that most participants believed to be in the active condition, which might have produced placebo effects. An active control group could account for these and improve generalizability. Additionally, the sample consisted only of healthy, male participants and focused only on a specific brain area. This decision was made to reduce variance in the results but hinders the generalizability. Also, the distance between the anode and cathodes was rather short, increasing the chance that the current propagates through the scalp.

The time-dependent change in the relation between EF magnitude and rsFC during stimulation only related to a small area and the analysis was explorative in nature. We tried to account for the explorative whole-brain analysis by using FWE correction, but our findings need further confirmation.

5. Conclusion

We used a 4 × 1 ring setup that is frequently used for HD-tDCS applications. Results showed an increase in rsFC between the rIFG-ptr and parts of the left PFC including the frontal pole, middle frontal gyrus, and IFG during, and directly following active but not sham stimulation. Findings also revealed substantial EF variability. Furthermore, an interaction between the duration of stimulation and EF magnitude on changes in rsFC was observed. While these findings need further validation, they emphasize the importance of individual EF models and individualized (HD-)tDCS protocols. One option to optimize protocols could be the adjustment of the current intensity to a target value in the area that is aimed to be stimulated.

Funding

This work was funded by the Deutsche Forschungsgemeinschaft (DFG, German Research Foundation e 269953372/GRK2150) and the START-Program of the Faculty of Medicine of the RWTH Aachen University. This work was supported by the Brain Imaging Facility, a Facility of the Interdisciplinary Centre for Clinical Research (IZKF) Aachen within the Faculty of Medicine at RWTH Aachen University.

Data availability

The research data supporting this study cannot be made publicly available because we do not have an ethics vote for sharing the data.

CRediT authorship contribution statement

Dario Müller: Conceptualization, Data curation, Formal analysis, Investigation, Methodology, Visualization, Writing – original draft, Writing – review & editing. **Ute Habel:** Funding acquisition, Investigation, Resources, Supervision, Writing – review & editing. **Edward S. Brodkin:** Investigation, Supervision, Writing – review & editing. **Benjamin Clemens:** Investigation, Supervision, Writing – review & editing. **Carmen Weidler:** Conceptualization, Data curation, Funding acquisition, Investigation, Supervision, Validation, Writing – review & editing.

Declaration of competing interest

The authors declare that they have no known competing financial interests or personal relationships that could have appeared to influence the work reported in this paper.

Appendix A. Supplementary data

Supplementary data to this article can be found online at https://doi.org/10.1016/j.brs.2023.11.012.

References

[1] Nitsche MA, Paulus W. Excitability changes induced in the human motor cortex by weak transcranial direct current stimulation. J Physiol 2000;527:633–9.
[2] Reed T, Cohen Kadosh R. Transcranial electrical stimulation (tES) mechanisms and its effects on cortical excitability and connectivity. J Inherit Metab Dis 2018;41:1123–30.
[3] Paulus W, Nitsche MA, Antal A. Application of transcranial electric stimulation (tDCS, tACS, tRNS): from motor-evoked potentials towards modulation of behaviour. Eur Psychol 2016;21:4–14.
[4] Liebetanz D, Nitsche MA, Tergau F, Paulus W. Pharmacological approach to the mechanisms of transcranial DC-stimulation-induced after-effects of human motor cortex excitability. Brain 2002;125:2238–47.
[5] Nitsche MA, et al. Pharmacological modulation of cortical excitability shifts induced by transcranial direct current stimulation in humans. J Physiol 2003;553:293–301.
[6] Stagg CJ, Nitsche MA. Physiological basis of transcranial direct current stimulation. Neuroscientist 2011;17:37–53.
[7] Palm U, Hasan A, Strube W, Padberg · Frank. tDCS for the treatment of depression: a comprehensive review. Eur Arch Psychiatr Clin Neurosci 2016;266:681–94.
[8] Parlikar R, et al. High definition transcranial direct current stimulation (HD-tDCS): a systematic review on the treatment of neuropsychiatric disorders. Asian J Psychiatr 2021;56.
[9] Mancuso LE, Ilieva IP, Hamilton RH, Farah MJ. Does transcranial direct current stimulation improve healthy working memory?: a meta-analytic review. J Cognit Neurosci 2016:28 1063–1089. https://doi.org/10.1162/jocn_a_00956. Preprint at.
[10] Edwards DJ, et al. Transcranial direct current stimulation and sports performance. Front Hum Neurosci 2017;11.
[11] Brunoni AR, et al. Digitalized transcranial electrical stimulation: a consensus statement. Clin Neurophysiol 2022;143:154–65.
[12] Aron AR, Robbins TW, Poldrack RA. Inhibition and the right inferior frontal cortex. Trends Cognit Sci 2004;8:170–7.
[13] Aron AR, Robbins TW, Poldrack RA. Inhibition and the right inferior frontal cortex: one decade on. Trends Cognit Sci 2014;18:177–85.
[14] Fan S, et al. Trans-diagnostic comparison of response inhibition in Tourette's disorder and obsessive-compulsive disorder. World J Biol Psychiatr 2018;19:527–37.
[15] Sofuoglu M, DeVito EE, Waters AJ, Carroll KM. Cognitive function as a transdiagnostic treatment target in stimulant use disorders. J Dual Diagn 2016;12:90–106.
[16] Goschke T. Dysfunctions of decision-making and cognitive control as transdiagnostic mechanisms of mental disorders: advances, gaps, and needs in current research. Int J Methods Psychiatr Res 2014;23(Suppl 1):41–57.
[17] Jacobson L, Koslowsky M, Lavidor M. tDCS polarity effects in motor and cognitive domains: a meta-analytical review. Exp Brain Res 2012;216:1–10.
[18] Batsikadze G, Moliadze V, Paulus W, Kuo MF, Nitsche MA. Partially non-linear stimulation intensity-dependent effects of direct current stimulation on motor cortex excitability in humans. J Physiol 2013;591:1987–2000.
[19] Samani MM, Agboada D, Kuo M-F, Nitsche MA. Probing the relevance of repeated cathodal transcranial direct current stimulation over the primary motor cortex for prolongation of after-effects. J Physiol 2020;598:805–16.
[20] Horvath JC, Vogrin SJ, Carter O, Cook MJ, Forte JD. Effects of a common transcranial direct current stimulation (tDCS) protocol on motor evoked potentials found to be highly variable within individuals over 9 testing sessions. Exp Brain Res 2016;234:2629–42.
[21] Müller D, Habel U, Brodkin ES, Weidler C. High-definition transcranial direct current stimulation (HD-tDCS) for the enhancement of working memory – a systematic review and meta-analysis of healthy adults. Brain Stimul 2022;15:1475–85.
[22] López-Alonso V, Cheeran B, Río-Rodríguez D, Fernández-Del-Olmo M. Inter-individual variability in response to non-invasive brain stimulation paradigms. Brain Stimul 2014;7:372–80.
[23] Vignaud P, Mondino M, Poulet E, Palm U, Brunelin J. Duration but not intensity influences transcranial direct current stimulation (tDCS) after-effects on cortical excitability. Neurophysiol Clin 2018;48:89–92.
[24] Ehrhardt SE, Filmer HL, Wards Y, Mattingley JB, Dux PE. The influence of tDCS intensity on decision-making training and transfer outcomes. J Neurophysiol 2021;125:385–97.
[25] Ammann C, Lindquist MA, Celnik PA. Response variability of different anodal transcranial direct current stimulation intensities across multiple sessions. Brain Stimul 2017;10:757–63.
[26] Opitz A, Paulus W, Will S, Antunes A, Thielscher A. Determinants of the electric field during transcranial direct current stimulation. Neuroimage 2015;109:140–50.
[27] Albizu A, et al. Machine learning and individual variability in electric field characteristics predict tDCS treatment response. Brain Stimul 2020;13:1753–64.
[28] Indahlastari A, et al. Individualized tDCS modeling predicts functional connectivity changes within the working memory network in older adults. Brain Stimul 2021;14:1205–15.
[29] Laakso I, Mikkonen M, Koyama S, Hirata A, Tanaka S. Can electric fields explain inter-individual variability in transcranial direct current stimulation of the motor cortex? Sci Rep 2019;9.
[30] Mikkonen M, Laakso I, Tanaka S, Hirata A. Cost of focality in TDCS: interindividual variability in electric fields. Brain Stimul 2020;13:117–24.
[31] Peña-Gómez C, et al. Modulation of large-scale brain networks by transcranial direct current stimulation evidenced by resting-state functional MRI. Brain Stimul 2012;5:252–63.

[32] Amadi U, Ilie A, Johansen-Berg H, Stagg CJ. Polarity-specific effects of motor transcranial direct current stimulation on fMRI resting state networks. Neuroimage 2014;88:155–61.
[33] Bouchard AE, et al. Concurrent transcranial direct current stimulation and resting-state functional magnetic resonance imaging in patients with gambling disorder. Brain Connect 2021;11:815–21.
[34] Wang X, et al. Dynamic influence of ongoing brain stimulation on resting state fMRI connectivity: a concurrent tDCS-fMRI study. 2018. 10.0/Linux-x86_64.
[35] Yaqub MA, Hong KS, Zafar A, Kim CS. Control of transcranial direct current stimulation duration by assessing functional connectivity of near-infrared spectroscopy signals. Int J Neural Syst 2022;32.
[36] Yuan K, et al. Individual electric field predicts functional connectivity changes after anodal transcranial direct-current stimulation in chronic stroke. Neurosci Res 2023;186:21–32.
[37] First MB, Williams JBW, Karg RS, Spitzer RL. SCID-5-CV: Structured clinical interview for DSM-5 disorders: clinician version. VA: American Psychiatric Association Publishing Arlington; 2016.
[38] Nieto-Castanon A. Handbook of functional connectivity magnetic resonance imaging methods in CONN. Hilbert Press; 2020.
[39] Andersson JLR, Hutton C, Ashburner J, Turner R, Friston K. Modeling geometric deformations in EPI time series. Neuroimage 2001;13:903–19.
[40] Friston KJ, et al. Spatial registration and normalization of images. Hum Brain Mapp 1995;3:165–89.
[41] Whitfield-Gabrieli S, Nieto-Castanon A, Ghosh S. Artifact detection tools (ART), vol. 7. Cambridge, MA: Release Version; 2011. p. 11.
[42] Power JD, et al. Methods to detect, characterize, and remove motion artifact in resting state fMRI. Neuroimage 2014;84:320–41.
[43] Nieto-Castanon A. Preparing fMRI data for statistical analysis. 2022. p. 13564. *arXiv preprint arXiv2210*.
[44] Calhoun VD, et al. The impact of T1 versus EPI spatial normalization templates for fMRI data analyses. 2017.
[45] Ashburner J. A fast diffeomorphic image registration algorithm. Neuroimage 2007;38:95–113.
[46] Ashburner J, Friston K. J. Unified segmentation. Neuroimage 2005;26:839–51.
[47] Friston KJ, Williams S, Howard R, Frackowiak RSJ, Turner R. Movement-related effects in fMRI time-series. Magn Reson Med 1996;35:346–55.
[48] Hallquist MN, Hwang K, Luna B. The nuisance of nuisance regression: spectral misspecification in a common approach to resting-state fMRI preprocessing reintroduces noise and obscures functional connectivity. Neuroimage 2013;82:208–25.
[49] Behzadi Y, Restom K, Liau J, Liu TT. A component based noise correction method (CompCor) for BOLD and perfusion based fMRI. Neuroimage 2007;37:90–101.
[50] Chai XJ, Castañón AN, Öngür D, Whitfield-Gabrieli S. Anticorrelations in resting state networks without global signal regression. Neuroimage 2012;59:1420–8.
[51] Worsley KJ, et al. A unified statistical approach for determining significant signals in images of cerebral activation. Hum Brain Mapp 1996;4:58–73.
[52] Chumbley J, Worsley K, Flandin G, Friston K. Topological FDR for neuroimaging. Neuroimage 2010;49:3057–64.
[53] Thielscher A, Antunes A, Saturnino GB. Field modeling for transcranial magnetic stimulation: a useful tool to understand the physiological effects of TMS?. In: Proceedings of the annual international conference of the IEEE engineering in medicine and biology society, EMBS 2015-november; 2015. p. 222–5.
[54] The MathWorks Inc. MATLAB version: 9.13.0 (R2022b). 2022. https://www.mathworks.com.
[55] Puonti O, et al. Accurate and robust whole-head segmentation from magnetic resonance images for individualized head modeling. Neuroimage 2020;219.
[56] Beaufort PA, Geuzaine C, Remacle JF. Automatic surface mesh generation for discrete models – a complete and automatic pipeline based on reparametrization. J Comput Phys 2020;417.
[57] Whitfield-Gabrieli S, Nieto-Castanon, Conn A. A functional connectivity toolbox for correlated and anticorrelated brain networks. Brain Connect 2012;2:125–41.
[58] Nieto-Castanon, Alfonso. CONN functional connectivity toolbox (RRID:SCR_009550). 2021. https://doi.org/10.56441/hilbertpress.2161.7292., Version 21.
[59] Penny WD, Friston KJ, Ashburner JT, Kiebel SJ, Nichols TE. Statistical parametric mapping the analysis of functional brain images. Elsevier; 2011.
[60] Desikan RS, et al. An automated labeling system for subdividing the human cerebral cortex on MRI scans into gyral based regions of interest. Neuroimage 2006;31:968–80.
[61] R Core Team. R: a language and environment for statistical computing. Preprint at, https://www.R-project.org/; 2022.
[62] Wickham H. ggplot2: elegant graphics for data analysis. Springer-Verlag New York; 2016.
[63] Hartwigsen G, et al. Perturbation of the left inferior frontal gyrus triggers adaptive plasticity in the right homologous area during speech production. Proc Natl Acad Sci U S A 2013;110:16402–7.
[64] Yaqub MA, Woo SW, Hong KS. Effects of HD-tDCS on resting-state functional connectivity in the prefrontal cortex: an fNIRS study. Complexity 2018;2018.
[65] Keeser D, et al. Prefrontal transcranial direct current stimulation changes connectivity of resting-state networks during fMRI. J Neurosci 2011;31:15284–93.
[66] Chang C, Glover GH. Time-frequency dynamics of resting-state brain connectivity measured with fMRI. Neuroimage 2009;50:81–98.
[67] Chiang Sharon, Vankov ER, Y. H. J. A. N. D. G. M. A. N. D. V. M. & H. Z. A. N. D. S. J. M. Temporal and spectral characteristics of dynamic functional connectivity between resting-state networks reveal information beyond static connectivity. PLoS One 2018;13:1–25.
[68] Woodward ND, Cascio CJ. Resting-state functional connectivity in psychiatric disorders. JAMA Psychiatr 2015;72:743–4.
[69] Hou JM, et al. Resting-state functional connectivity abnormalities in patients with obsessive–compulsive disorder and their healthy first-degree relatives. J Psychiatr Neurosci 2014;39:304–11.
[70] Guo H, et al. Resting-state functional connectivity abnormalities in first-onset unmedicated depression. Neural Regen Res 2014;9:153.
[71] Antonenko D, et al. Towards precise brain stimulation: is electric field simulation related to neuromodulation?. 2019. https://doi.org/10.1016/j.brs.2019.03.072.
[72] Hassanzahraee M, Nitsche MA, Zoghi M, Jaberzadeh S. Determination of anodal tDCS duration threshold for reversal of corticospinal excitability: an investigation for induction of counter-regulatory mechanisms. Brain Stimul 2020;13:832–9.
[73] Hassanzahraee, M., Nitsche, M. A., Zoghi, M. & Jaberzadeh, S. Determination of anodal tDcS intensity threshold for reversal of corticospinal excitability: an investigation for induction of counter-regulatory mechanisms. Sci Rep | 10, 16108 (123AD)..
[74] Hsu TY, Juan CH, Tseng P. Individual differences and state-dependent responses in transcranial direct current stimulation. Front Hum Neurosci 2016;10:233364.
[75] Dubreuil-Vall L, Chau P, Ruffini G, Widge AS, Camprodon JA. tDCS to the left DLPFC modulates cognitive and physiological correlates of executive function in a state-dependent manner. Brain Stimul 2019;12:1456–63.
[76] Mizutani-Tiebel Y, et al. Differences in electric field strength between clinical and non-clinical populations induced by prefrontal tDCS: a cross-diagnostic, individual MRI-based modeling study. Neuroimage Clin 2022;34.
[77] Birn RM, et al. The effect of scan length on the reliability of resting-state fMRI connectivity estimates. Neuroimage 2013;83:550–8.